Core-shell Au/CeO_2 nanoparticles supported in UiO-66 beads exhibiting full CO conversion at 100 ˚C

Received 00th January 20xx,
Accepted 00th January 20xx

DOI: 10.1039/x0xx00000x

www.rsc.org/

A. Yazdi,[a] A. Abo Markeb,[b] L. Garzón-Tovar,[a] J. Patarroyo,[a] J. Moral-Vico,[b] A. Alonso,[*,b] A. Sánchez,[b] N. Bastus,[a] I. Imaz,[a] X. Font,[b] V. Puntes,[*,a,c,d] and D. Maspoch[*,a,d]

Hybrid core-shell Au/CeO_2 nanoparticles (NPs) dispersed in UiO-66 shaped into microspherical beads are created using the spray-drying continuous-flow method. The combined catalytic properties of nanocrystalline CeO_2 and Au in a single particle and the support and protective function of porous UiO-66 beads make the resulting composites showing good performances as catalysts for CO oxidation (T_{50} = 72 ˚C; T_{100} = 100˚C) and recyclability.

Long-term exposure to carbon monoxide gas is a cause of lethal damage to humans and animals.[1] Only in 2014, 6381 kilotons of CO were emitted in the world, mainly from transportation, power plants and industrial activities[2]. To date, one of the most efficient solutions for mitigating CO emissions to atmosphere is its catalytic oxidation to CO_2.[3, 4] Good-performance catalysts for CO oxidation are metal nanoparticles (NPs) such as Au, Pd, Pt and Ru NPs.[5-8] These NPs are usually supported on/in zeolites,[9] activated carbon,[10] and metal oxides, including alumina,[11] mesoporous silica,[12] ceria,[13-17] zirconia,[18] titania,[19] and iron oxides.[3] These supports avoid NP aggregation and, eventually, enhance the catalytic activity of NPs. A remarkable case is the use of nanocrystalline CeO_2 to support Au NPs.[20, 21] In this particular composite, CeO_2 acts as an active support that enhances the catalytic performance of Au NPs for CO oxidation. Indeed, because CeO_2 has a high oxygen storage and release capacity[22] and facile oxygen vacancy formation, its surface can be easily enriched with oxygen vacancies so that Au NPs can strongly bind to these vacancies.[23,24] Also, the oxygen vacancies in CeO_2 can create Ce^{3+} ions, opening a new CO oxidation pathway by O_2 adsorbed on Au-Ce^{3+} bridge site.[23] Moreover, the interaction between the ceria and the metal NPs can prevent reorganization of the metallic atoms under operating conditions. [22]

Inspired by these latter results, herein we show a fast method that enables integrating pre-designed core-shell Au/CeO_2 NPs[25-27] in metal-organic frameworks (MOFs). Recently, MOFs have attracted much attention as new porous supports for catalytic NPs due to their exceptionally high surface areas, structural diversity and tailorable pore chemical functionalities.[28] For CO oxidation, Xu *et al.* have shown that ZIF-8 MOF can support Au NPs to fully oxidize CO at a temperature of 225 ˚C.[29] Similarly, Pd and Pt NPs and hybrid Pd/Pt NPs supported on MIL-101, ZIF-8, UiO-67 and UiO-66 MOFs showed full CO conversion at temperatures ranging from 120 ˚C to 200 ˚C (Table 1).[30-33] In this work, we combine the catalytic properties for CO oxidation of both nanocrystalline CeO_2 and Au counterparts in a single particle entity, which is supported in UiO-66 beads using the spray-drying continuous-flow method. This method allows the simultaneously synthesis and shaping of MOF beads while encapsulating the pre-synthesized NPs in a fast, continuous one-step process.[34-36]

Table 1 Inorganic nanoparticles supported on MOFs for CO oxidation.

Catalyst	*NPs w.t.%*	*T_{50} (˚C)*	*T_{100} (˚C)*	*ref.*
UiO-66@Au/CeO_2	7	72	100	this work
UiO-66@Au/CeO_2	5.5	82	110	this work
UiO-67@Pt	5	100	120	33
MIL-101@Pt/Pd		160	175	30
MIL-101@Pt		160	175	30
UiO-66@Au/CeO_2	2.8	98	180	this work
UiO-66@Pt	2	160	180	32
MIL-101@Pd		185	200	30
ZIF-8@Pt	2	170	200	31
ZIF-8@Au	5	170	225	29
UiO-66		369	440	this work

[a] *Catalan Institute of Nanoscience and Nanotechnology (ICN2), CSIC and The Barcelona Institute of Science and Technology Campus UAB, Bellaterra, 08193 Barcelona, Spain. E-mail: victor.puntes@icn2.cat; daniel.maspoch@icn2.cat*
[b] *Department of Chemical, Biological and Environmental Engineering, Escola d'Enginyeria, Universitat Autònoma de Barcelona, 08193 Bellaterra, Spain. E-mail: Amanda.Alonso@uab.cat*
[c] *Vall, d'Hebron Institut de Recerca (VHIR), 08035, Barcelona, Spain.*
[d] *ICREA, Pg. Lluís Companys 23, 08010 Barcelona, Spain*
† Footnotes relating to the title and/or authors should appear here.
Electronic Supplementary Information (ESI) available. See DOI: 10.1039/x0xx00000x

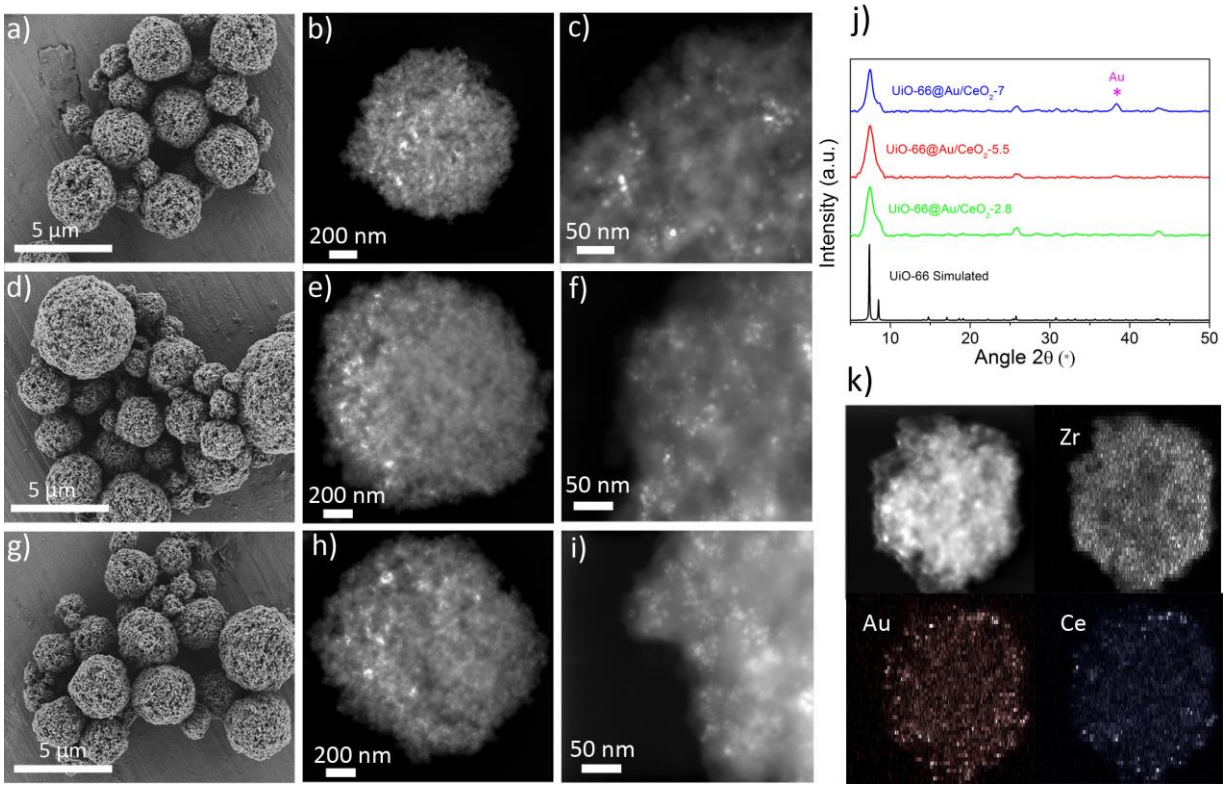

Fig. 1 (a-i) Representative FE-SEM and HAADF-STEM images of UiO-66@Au/CeO_2-2.8 (a-c), UiO-66@Au/CeO_2-5.5 (d-f) and UiO-66@Au/CeO_2-7 (g-i). (j) XRPD patterns of UiO-66@Au/CeO_2-2.8 (green), UiO-66@Au/CeO_2-5.5 (red) and UiO-66@Au/CeO_2-7 (blue) in comparison to the simulated pattern for UiO-66 (black). (k) Elemental mapping (Zr, Ce and Au) of the composite UiO-66@Au/CeO_2-2.8.

Our method started with the synthesis of core-shell Au/CeO_2 (Ce:Au = 1:1) NPs in water following the simultaneous reduction/oxidation of Au and Ce precursors (ESI†). Synthesized NPs had an average particle size of 9.6 ± 2.0 nm and Au core size of 4.2 ± 1.2 nm (Fig. S1, ESI†). Then, they were functionalized with PVP, allowing them to be transferred from water to dimethylformamide (DMF). This step enables the dispersion of Au/CeO_2 NPs in the solvent needed for synthesizing the UiO-66 beads. Afterwards, 100 mg of terephthalic acid, 3 mL of acetic acid, 4 ml of Au/CeO_2 NPs (concentration = 1 mg/mL) and 280 µL of $Zr(OPr^n)_4$ were sequentially mixed in 40 ml DMF. Note here that $ZrCl_4$, which is the common salt used to synthesize UiO-66, was replaced by $Zr(OPr^n)_4$ because of the dissolution of CeO_2 in the acidic precursor solution when $ZrCl_4$ is utilized (Fig. S2, ESI†).[37] This mixture was injected into a coil flow reactor at a feed rate of 2.4 ml.min^{-1} at 115 ˚C. The resulting pre-heated solution was then spray dried at 180 ˚C and a flow rate of 336 ml/min using a spray cap with a 0.5 mm diameter hole. The collected solid was dispersed in DMF and washed twice with DMF and ethanol.[34]

A final step involved its calcination at 250˚C overnight in the presence of air. This calcination process facilitates the removal of PVP from the surface of Au/CeO_2 NPs. It also enhances the interfacial interaction of Au and CeO_2 and increases the crystallinity of CeO_2, which leads to an enhancement of oxygen generation/storage capacity of ceria.[38-40]

Field-emission scanning electron microscopy (FE-SEM) of the calcinated powder revealed the formation of spherical beads (average size = 3.4 ± 1.8 µm) formed by the assembly of nanocrystals of UiO-66 (Fig. 1a). X-ray powder diffraction (XRPD) indicated that the beads were pure crystalline UiO-66 (Fig. 1j). Fig. 1b,c shows high angle annular dark field scanning transmission electron microscopy (HAADF-STEM) of these beads, confirming the encapsulation of well-dispersed Au/CeO_2 NPs inside them. In addition, energy dispersive X-ray spectroscopy (EDX) mapping of the beads showed the homogeneous distribution of Au and Ce inside the beads (Fig. 1k). The content of Au/CeO_2 in this composite was estimated by digesting the powder in a mixture of concentrated HCl and HNO_3 and analysed by inductively coupled plasma optical emission spectrometry (ICP-OES), from which a Au/CeO_2 content of 2.8 % (Ce: 1.28 %, Au: 1.31 %) in the composite (hereafter, UiO-66@Au/CeO_2-2.8) was determined. The comparison of this value to the initial percentage of Au/CeO_2 NPs added into the UiO-66 precursor solution leads to an encapsulation yield of 92 %, confirming the efficiency of the spray drying method for incorporating Au/CeO_2 NPs into the UiO-66 beads. Finally, the adsorption capacity of UiO-66@Au/CeO_2-2.8 was determined. N_2 physical adsorption measurements showed a measured Brunauer Emmet Teller (BET) surface area (A_{BET}) of 1095 m^2/g (Fig. S3a, ESI†), very close to that of pristine UiO-66 superstructures.[37]

The catalytic activity of the UiO-66@Au/CeO_2-2.8 in CO oxidation was evaluated by the temperature-programed oxidation method. The catalytic oxidation of CO was carried out in a fixed bed column reactor with dimensions of 9.0 cm in length and 0.5 cm in inner diameter set in a controlled temperature oven. 50 mg of the catalyst was packed into the column, and a mixture of gases consisting of 1 % CO, 21 % O_2 and 78 % N_2 was allowed to pass through the column reactor at a constant flow rate of 100 ml/min. After that, the catalyst was heated up to the desired temperature and maintained until a steady state was achieved. Within this interval of time, set of samples of the outlet gas were withdrawn and analyzed to determine the CO converted.

In an initial step, the catalytic activity of UiO-66 beads without Au/CeO_2 NPs was measured as a control reaction. As expected, UiO-66 beads showed no conversion of CO to CO_2 up to 200 ˚C, and full conversion took place at 440 ˚C (Fig. S4, ESI†). On the contrary, the catalytic activity of UiO-66@Au/CeO_2-2.8 was remarkably enhanced. As is shown in Fig. 2a, this composite showed a CO conversion starting at room temperature and exhibited a 50 % (T_{50}) and 100 % (T_{100}) CO conversion at temperatures of 98 ˚C and 180˚C, respectively (Table 1).

It is known that, if no aggregation occurs, higher loading of NPs tends to increase the catalytic activity of this class of supported composites. To this end, we systematically synthesized a series of composites in which we increased the added amount of Au/CeO_2 NPs dispersion (1 mg/mL) in the precursor solution to 8.5 mL, 12 mL and 16 mL. Again, FESEM and HAADF-STEM images revealed the formation of beads containing Au/CeO_2 NPs for all samples (Fig. 1d-i). However, the latter sample was discarded because it showed the presence of a high amount of non-encapsulated Au/CeO_2 NPs together with the beads as well as lower crystallinity of UiO-66 (Fig. S5, ESI†). For the first two compositions, XRPD patterns confirmed the formation of UiO-66 (Fig. 1j), from which Au/CeO_2 contents of 5.5 % (Ce: 2.48 %, Au: 2.50 %) and 7 % (Ce: 3.22 %, Au: 3.18 %) in the composites (hereafter, UiO-66@Au/CeO_2-5.5 and UiO-66@Au/CeO_2-7) were determined. These amounts correspond to 91 % and 74 % of encapsulation efficiency for UiO-66@Au/CeO_2-5.5 and UiO-66@Au/CeO_2-7, respectively. Finally, N_2 physical adsorption measurements confirmed that both composites are porous, showing measured BET surface areas of 1070 and 870 m^2/g (Fig. S3b,c, ESI†).

Ensuing temperature-programed oxidation measurements confirmed a clear improvement of CO conversion for both new composites, achieving lower T_{50} and T_{100} values by increasing the percentage of Au/CeO_2 NPs (Fig 2a). In the case of UiO-66@Au/CeO_2-5.5, T_{50} and T_{100} were found to be 82 ˚C and 110 ˚C, respectively. For UiO-66@Au/CeO_2-7, these temperatures decreased down to 72 ˚C and 100 ˚C. Remarkably, in this latter case, a CO conversion of 3.8 % was achieved at room temperature. Moreover, for this latter reaction, the activation energy was found to be 40.2 kJ/mol, whereas the turnover frequencies (TOF) values at temperatures of 30, 50, 75 and 100 ºC were 10, 39, 106 and 204 h^{-1}, respectively (for comparison

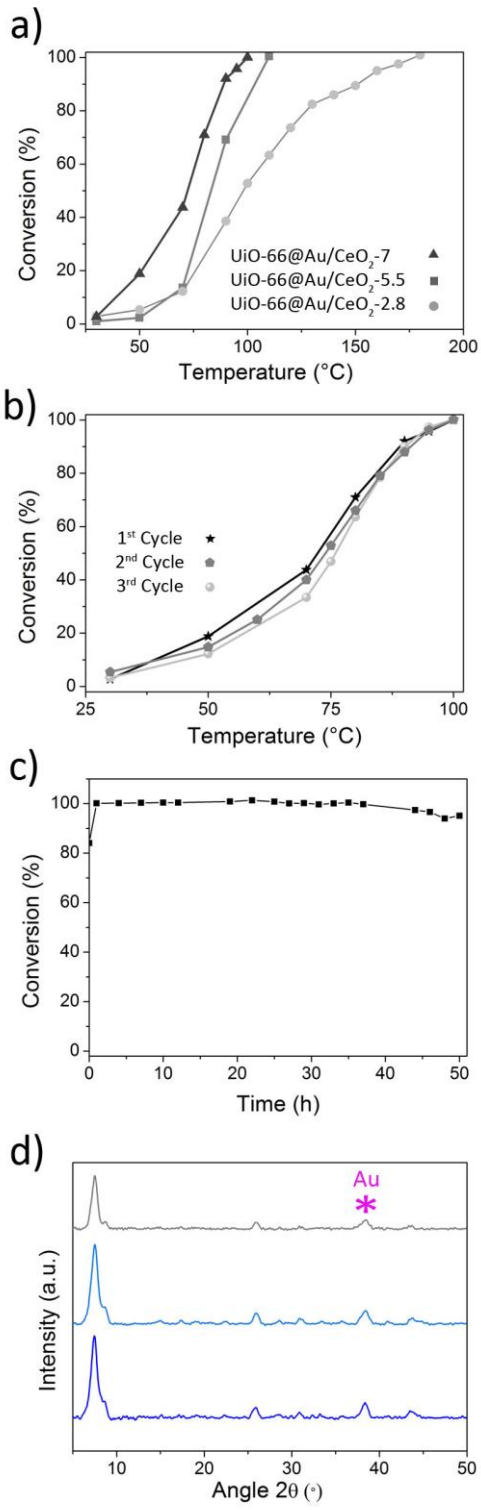

Fig. 2 (a) CO conversion rate as a function of reaction temperature for UiO-66@Au/CeO_2-2.8, UiO-66@Au/CeO_2-5.5 and UiO-66@Au/CeO_2-7. (b) CO conversion rate as a function of reaction temperature for three consecutive cycles over the UiO-66@Au/CeO_2-7 composite. (c) CO conversion rate at 100 ºC for 12 hours over the UiO-66@Au/CeO_2-7 composite. (d) XRPD patterns of as-synthesized UiO-66@Au/CeO_2-7 (blue) and after after three temperature-programed cycles (light blue) and 50 hours of continuous CO conversion (grey).

purposes, TOF values of other reported catalysts based on Au NPs are given in Table S1, ESI†).

Finally, the recyclability of these composites was evaluated using the composite UiO-66@Au/CeO_2-7 that shows the lower T_{100}. Initially, we performed three cycles of catalysis without detecting any loss of activity (Fig. 2b). After these cycles, the stability of UiO-66@Au/CeO_2-7 was analyzed by XRPD that showed a complete retention of the crystallinity of UiO-66 (Fig. 2d), as also confirmed by its unaffected surface area (A_{BET} = 850 m^2/g). Similarly, no sign of NP sintering or aggregation and alteration of the morphology of the beads was observed by STEM and FE-SEM (Fig. S6, ESI†). Then, the catalytic activity of UiO-66@Au/CeO_2-7 sample was also studied during a longer period of time. For this, the conversion of CO was followed in continue at 100 ℃ during 50 hours, from which it was not observed any loss of activity during the first 37 hours and a slight decrease of activity (5 %) after 50 hours (Fig. 2c). We attributed this decrease in catalytic activity to a loss of crystallinity of UiO-66 (Fig. 2d) and its porosity capabilities (A_{BET} = 670 m^2/g).

In conclusion, we have described the formation of a new composite based on the entrapment and dispersion of core-shell Au/CeO_2 NPs into microsized spherical, porous UiO-66 beads using the spray-drying continuous-flow method. The combination of nanocrystalline CeO_2 and Au allows accessing to CO conversion T_{50} and T_{100} as low as 72 ℃ and 100 ℃. These values are to our knowledge one of the lowest CO conversion temperatures achieved using catalysts based on NPs supported on MOFs. In addition, UiO-66 provides enough protection to avoid NP sintering/aggregation. We consider this method as a general approach for making composites consisting of functional NPs dispersed in MOFs already shaped into spherical beads, as demonstrated by the fact that other composites made of Pd NPs dispersed into UiO-66 beads (Fig. S7, ESI†) were also fabricated and tested for CO oxidation.

Acknowledgements

This work was supported by the Spanish MINECO (projects PN MAT2015-65354-C2-1-R and MAT2015-70725-R), the Catalan AGAUR (projects 2014-SGR-80 and 2014-SGR-612), and the ERC under the EU FP7 (ERC-Co 615954). N.G.B. thanks the MINECO for her RyC grant RYC-2012- 10991 and the financial support by the European Commission Seventh Framework Program (FP7) through the Marie Curie Career Integration Grant (322153-MINE). ICN2 acknowledges the support of the Spanish MINECO through the Severo Ochoa Centres of Excellence Programme, under Grant SEV-2013-0295.

Notes and references

1. R. A. Jones, J. A. Strickland, J. A. Stunkard and J. Siegel, *Toxicol. Appl. Pharmacol.*, 1971, **19**, 46-53.
2. *Environment and Climate Change Canada Canadian Environmental Sustainability Indicators: Air Pollutant Emissions. Available at: http://www.ec.gc.ca/indicateurs-indicators/default.asp?lang=en&n=E79F4C12-1.* , 2016.
3. L. Liu, F. Zhou, L. Wang, X. Qi, F. Shi and Y. Deng, *J. Catal.*, 2010, **274**, 1-10.
4. B. Qiao, A. Wang, X. Yang, L. F. Allard, Z. Jiang, Y. Cui, J. Liu, J. Li and T. Zhang, *Nat. Chem.*, 2011, **3**, 634-641.
5. M. S. Chen, Y. Cai, Z. Yan, K. K. Gath, S. Axnanda and D. W. Goodman, *Surf. Sci.*, 2007, **601**, 5326-5331.
6. J. Wang, Z. Wang and C.-J. Liu, *Appl. Mater. Interfaces*, 2014, **6**, 12860-12867.
7. P. J. Berlowitz, C. H. F. Peden and D. W. Goodman, *J. Phys. Chem.*, 1988, **92**, 5213-5221.
8. E. M. C. Alayon, J. Singh, M. Nachtegaal, M. Harfouche and J. A. van Bokhoven, *J. Catal.*, 2009, **263**, 228-238.
9. W. Han, P. Zhang, Z. Tang and G. Lu, *Process Saf. Environ. Prot.*, 2014, **92**, 822-827.
10. L. Wang, Y. Zhang, Y. Lou, Y. Guo, G. Lu and Y. Guo, *Fuel Process. Technol.*, 2014, **122**, 23-29.
11. A. S. Ivanova, E. M. Slavinskaya, R. V. Gulyaev, V. I. Zaikovskii, O. A. Stonkus, I. G. Danilova, L. M. Plyasova, I. A. Polukhina and A. I. Boronin, *Appl. Catal., B*, 2010, **97**, 57-71.
12. H. Wang and C.-j. Liu, *Appl. Catal., B*, 2011, **106**, 672-680.
13. A. E. R. S. Khder, H. M. A. Hassan, M. A. Betiha, K. S. Khairou and A. A. Ibrahim, *Reac. Kinet. Mech. Cat.*, 2014, **112**, 61-75.
14. D. Zhang, X. Du, L. Shi and R. Gao, *Dalton Trans.*, 2012, **41**, 14455-14475.
15. W. Liu, X. Liu, L. Feng, J. Guo, A. Xie, S. Wang, J. Zhang and Y. Yang, *Nanoscale*, 2014, **6**, 10693-10700.
16. D. Zhang, Y. Qian, L. Shi, H. Mai, R. Gao, J. Zhang, W. Yu and W. Cao, *Catal. Commun.*, 2012, **26**, 164-168.
17. W. Liu, T. Deng, L. Feng, A. Xie, J. Zhang, S. Wang, X. Liu, Y. Yang and J. Guo, *CrystEngComm*, 2015, **17**, 4850-4858.
18. C. M. Olmos, L. E. Chinchilla, J. J. Delgado, A. B. Hungría, G. Blanco, J. J. Calvino and X. Chen, *Catal. Lett.*, 2015, **146**, 144-156.
19. J. Wang, S. A. Kondrat, Y. Wang, G. L. Brett, C. Giles, J. K. Bartley, L. Lu, Q. Liu, C. J. Kiely and G. J. Hutchings, *ACS Catalysis*, 2015, **5**, 3575-3587.
20. S. Carrettin, P. Concepcion, A. Corma, J. M. Lopez Nieto and V. F. Puntes, *Angew. Chem. Int. Ed.*, 2004, **43**, 2538-2540.
21. M. Centeno, T. Ramírez Reina, S. Ivanova, O. Laguna and J. Odriozola, *Catalysts*, 2016, **6**, 158.
22. N. J. Divins, I. Angurell, C. Escudero, V. Perez-Dieste and J. Llorca, *Science*, 2014, **346**, 620-623.
23. H. Y. Kim, H. M. Lee and G. Henkelman, *J. Am. Chem. Soc.*, 2012, **134**, 1560-1570.
24. C. Zhang, A. Michaelides and S. J. Jenkins, *PCCP*, 2011, **13**, 22-33.
25. T. Mitsudome, M. Yamamoto, Z. Maeno, T. Mizugaki, K. Jitsukawa and K. Kaneda, *J. Am. Chem. Soc.*, 2015, **137**, 13452-13455.
26. F. Zhu, G. Chen, S. Sun and X. Sun, *J. Mater. Chem. A*, 2013, **1**, 288-294.
27. Y. H. Qu, F. Liu, Y. Wei, C. L. Gu, L. H. Zhang and Y. Liu, *Appl. Surf. Sci.*, 2015, **343**, 207-211.
28. P. Falcaro, R. Ricco, A. Yazdi, I. Imaz, S. Furukawa, D. Maspoch, R. Ameloot, J. D. Evans and C. J. Doonan, *Coord. Chem. Rev.*, 2016, **307, Part 2**, 237-254.
29. H.-L. Jiang, B. Liu, T. Akita, M. Haruta, H. Sakurai and Q. Xu, *J. Am. Chem. Soc.*, 2009, **131**, 11302-11303.
30. A. Aijaz, T. Akita, N. Tsumori and Q. Xu, *J. Am. Chem. Soc.*, 2013, **135**, 16356-16359.

31. G. Lu, S. Li, Z. Guo, O. K. Farha, B. G. Hauser, X. Qi, Y. Wang, X. Wang, S. Han, X. Liu, J. S. DuChene, H. Zhang, Q. Zhang, X. Chen, J. Ma, S. C. Loo, W. D. Wei, Y. Yang, J. T. Hupp and F. Huo, *Nat. Chem.*, 2012, **4**, 310-316.
32. W. Zhang, G. Lu, C. Cui, Y. Liu, S. Li, W. Yan, C. Xing, Y. R. Chi, Y. Yang and F. Huo, *Adv. Mater.*, 2014, **26**, 4056-4060.
33. G.-l. Zhuang, J.-q. Bai, X. Zhou, Y.-f. Gao, H.-l. Huang, H.-q. Cui, X. Zhong, C.-L. Zhong and J.-g. Wang, *Eur. J. Inorg. Chem.*, 2017, **2017**, 172-178.
34. L. Garzon-Tovar, M. Cano-Sarabia, A. Carne-Sanchez, C. Carbonell, I. Imaz and D. Maspoch, *React. Chem. Eng.*, 2016, **1**, 533-539.
35. A. Carné-Sánchez, I. Imaz, M. Cano-Sarabia and D. Maspoch, *Nat. Chem.*, 2013, **5**, 203-211.
36. J. P.-C. L. Garzon-Trovar, I. Imaz, D. Maspoch, *Adv. Funct. Mater.*, 2017, DOI: 10.1002/adfm.201606424.
37. B. Rungtaweevoranit, J. Baek, J. R. Araujo, B. S. Archanjo, K. M. Choi, O. M. Yaghi and G. A. Somorjai, *Nano Lett.*, 2016, **16**, 7645-7649.
38. B. He, Q. Zhao, Z. Zeng, X. Wang and S. Han, *J. Mater. Sci.*, 2015, **50**, 6339-6348.
39. L. Zhou, X. Li, Z. Yao, Z. Chen, M. Hong, R. Zhu, Y. Liang and J. Zhao, *Sci. Rep.*, 2016, **6**, 23900.
40. Y. Liu, H.-S. Chen, J. Li and P. Yang, *RSC Adv.*, 2015, **5**, 37585-37591.